Journal of Materials Chemistry C

Accepted Manuscript

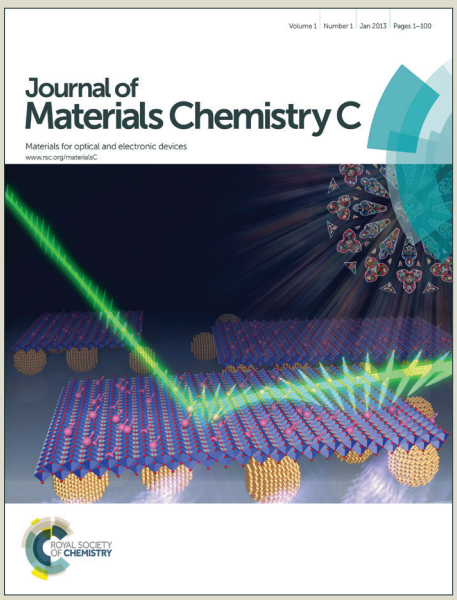

ROYAL SOCIETY OF CHEMISTRY

www.rsc.org/materialsC

Template-free synthesis of vertically aligned crystalline indium oxide nanotube arrays by pulsed Argon flow in tube-in-tube chemical vapor deposition system

*Kavita Yadav, B R Mehta and J P Singh**

Department of Physics, Indian Institute of Technology Delhi, Hauz Khas, New Delhi-110016, India

*E-mail: jpsingh@physics.iitd.ac.in

Abstract

Vertically aligned crystalline indium oxide (IO) nanotube arrays without using any special templates or expensive epitaxial substrates were synthesized on Si (100) substrates by tube-in-tube horizontal chemical vapor deposition (CVD) system. The pulsed flow of argon (Ar) gas in rectangular pulse mode appears to be a key factor in deciding the steady state of local vapor flux which further decides the growth alignment and yield of IO nanotubes.The dimensional distribution of IO nanotubes was simply controlled by varying the pulse width of Ar gas flow rate. This strategy of controlling dimensions and vertical alignment for making 1-D nanostructures may find potential applications in back electrodes photoelectrochemical cells, field emitters and solar cells.

Keywords: Chemical vapor deposition, pulsed flow, indium oxide, Vertical nanotubes.

Introduction

One dimensional (1-D) nanostructures have become the focus of intensive investigations in recent years, in particular vertically aligned 1-D nanostructures. The 1-D nanostructures could potentially provide an attractive solution to attain ultrahigh density advanced nanoscale devices and 3-D nanocircuitries. Controlled growth with well aligned direction is critical to realize and maximize the true potential of these nanostructures in advanced nanoelectronics and optoelectronics applications. Gan*et al.*[1] have prepared vertically aligned In_2O_3nanorod arrays (NRAs) on fluorine doped tin oxide (FTO) substrates via electrochemical assembly process and showed that these vertically aligned In_2O_3 NRAs are very promising for photoelectrochemical cells. In another work, growth of vertically aligned tin-doped indium oxide (ITO) nanowire arrays on ITO/yttrium stabilized zirconia substrates was reported by Wan *et al*.[2]These vertically aligned ITO nanowire arrays have shown to be an excellent field emitters. Varghese *et al.*[3] have reported the fabrication of transparent titania nanotube arrays on transparent conducting oxide glass using electrochemical approach which can be used for highly efficient solar cells. The highly ordered titania nanotube arrays have been shown to enhance the efficiencies of both charge collection and light harvesting. In addition to the advantages of vertically aligned nanostructures such as IO nanorods, ITO nanowires and IO nanowires,[1,2,4] nanotubes have their own particular advantages and unique applications because of their large surface-to-volume ratio and large pore volume. Applications of nanotubular morphology in various fields such as photoelectrochemical sensing,[5, 6]flexible bio-sensitized solar cell,[7]photoelectrochemicalwater splitting and sensitised solar cell[8] have been reported. It is important to note that growth of well aligned nanotube arrays are quite limited and are only possible by using anodization method,[9] surface-induced epitaxial growth[10] and templates method.[11-13] These reported manufacturing processes are complex and include expensive epitaxial substrate and inexpugnable templates. Sometimes, during removal of hard templates, the nanostructures get damaged. Therefore, there is a need of an

economical, facile and effective approach to fabricate well aligned vertically aligned nanotube arrays.

Indium oxide (IO), a well known n-type semiconductor with wide band gap (~3.6 eV) and high transparency in visible region (~90%) is suitable for a number of nanoelectronics and optoelectronics devices such as solar cells,[14] field effect transistors,[15] lithium ion batteries,[16] nanoscale biosensors,[17] gas sensors and photocatalysis.[18, 19] In the present research work, we report the fabrication of vertically aligned IO nanotube arrays without using any template or expensive epitaxial substrates. The IO nanotube arrays were synthesized by using pulsed Ar gas flow in a tube-in-tube chemical vapor deposition (CVD) system. Furthermore, tuning of nanotubes' dimensions is shown to be possible by varying the pulse width of Ar gas flow. We consider that it might provide a novel way of growing vertically aligned IO nanotube arrays with tunable dimensions.

Experimental details

Vertically aligned crystalline IO nanotubes were synthesized by using CVD method in the presence of reducing reagent ethanol. The growth was carried out by a single zone horizontal tube-in-tube furnace maintained at 1000 ℃and one atmospheric pressure. The schematic diagram of the tube-in-tube setup is shown in Fig. 1. The system was purged with Ar gas at a rate of 200 sccm for 20 minutes. The IO+ C (1:1) mixed powder and gold coated (~8 nm) Si substrates were placed inside the one end closed, smaller quartz tube (inner tube) in a pre-heated horizontal tube furnace. The precursor positioned upstream at 970 ℃ and substrate downstream at 920 ℃ temperature inside the quartz tube. A small reservoir (200 ml) of ethanol was placed at 120 ℃ during the growth and Ar gas bubbled through ethanol, carry ethanol vapors to the reaction zone. The total growth time was two hours. A series of

experiments were done with varying the Ar gas flow rate in order to grow vertically aligned IO nanotubes.

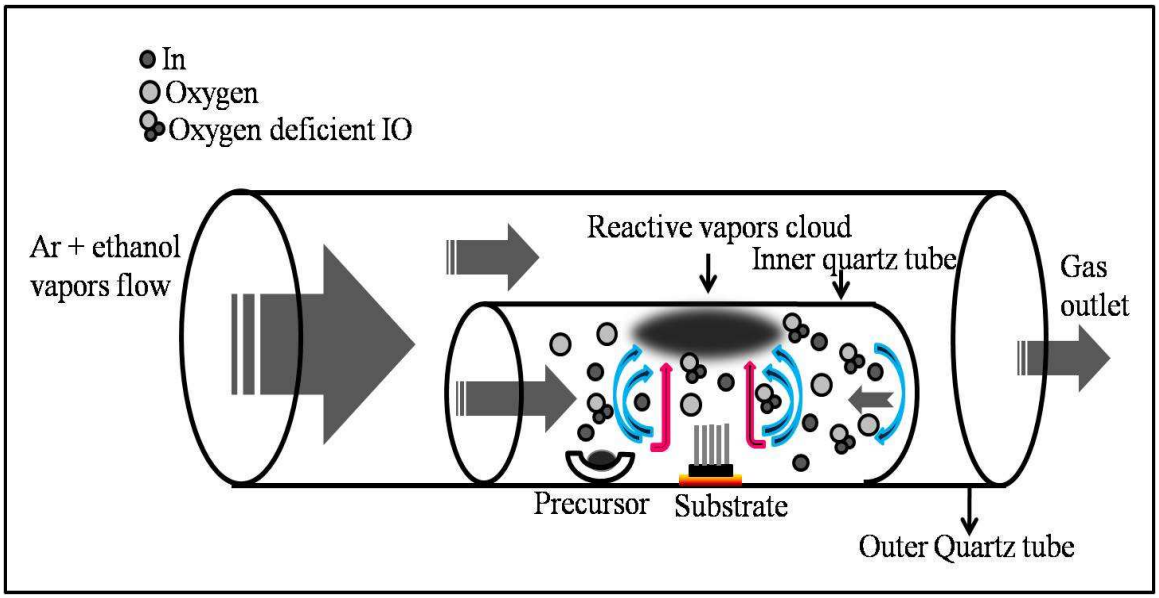

Fig. 1 Schematic diagram showing the gas flow dynamics in one end closed inner quartz tube in tube-in-tube CVD system for growth of vertical aligned IO nanotubes.

The characterization was done using glancing angle X-ray diffraction (GAXRD) with 1° glancing angle (Phillips X'Pert, PRO-PW 3040 diffractometer), field effect scanning electron microscope (FESEM; FEI Quanta 3D FEG) and a high resolution transmission electron microscope (HRTEM; Tecnai G20-Stwin 200 kV). Scanning transmission electron microscope (STEM) in nanoprobe mode with energy dispersive X-ray (EDX) facility was used to determine the position dependent stoichiometry and line profile of IO nanotubes.The photoluminescence (PL) and Raman measurements were taken using Horiba JobinYvon Lab RAM (HR 800 Evolution) system. For PL measurements, He–Cd laser with 325 nmwavelengthand 30 mW power was used as an excitation source.For Raman measurements Ar ion laser of 514 nm wavelength and 50 mW power was used. The integration time was set at 10 s during the Raman measurements.

Results and discussion

Here, we make use of different flow rate of carrier gas Ar to modulate the local flux of reactive vapors during the growth. The Ar gas flow rate for growth of well aligned vertical IO nanotube arrays in a tube-in-tube CVD system was optimized. A series of samples were fabricated under varying Ar gas flow rate during the subsequent growth of IO while the other deposition parameters were kept constant. Fig. 2(a-c) show the FESEM images of IO samples prepared under constant Ar gas flow rate values of 50, 100 and 200 sccm, respectively. For smaller gas flow rates (50 sccm and 100 sccm), particles with undefined shape were grown as shown in Fig. 2a and b. On the other hand, for the gas flow rate of 200 sccm,

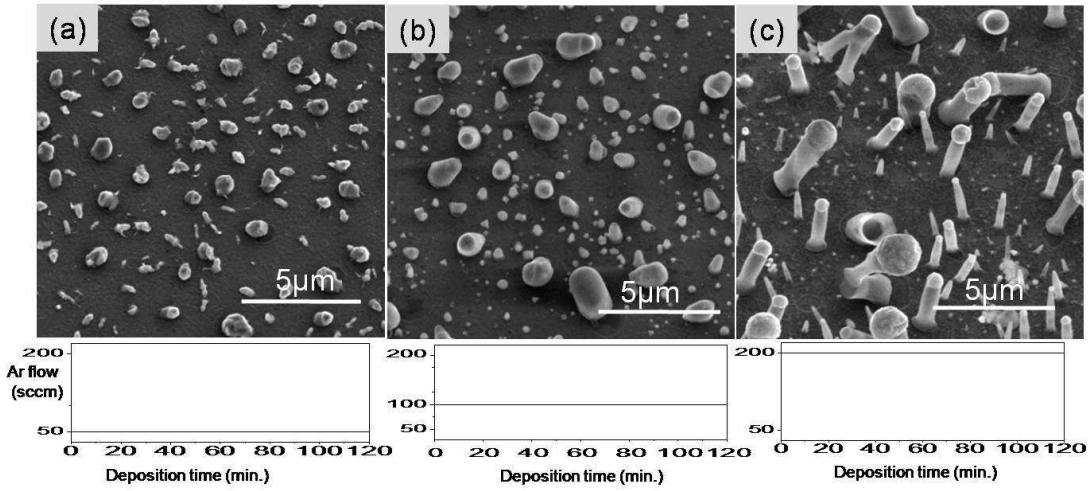

Fig. 2 FESEM micrograph of IO growth for (a) 50 sccm, (b) 100 sccm, (c) 200 sccm. The constant flow of Ar gas during complete growth time is shown graphically below the respective FESEM images.

nanotubes (later confirmed by TEM) were grown as shown in Fig. 2c. From now onwards, this sample will be referred as sample IO-0. The observations reveal that the reactive vapor flux transported byAr carrier gas with 50 sccm and 100 sccm flow rate was insufficient for growth of nanotubes. But for 200 sccm gas flow rate, the vapor flux was sufficient for nanotubes growth. It is important to note that the nanotubes grown in samples IO-0 have a wider distribution of diameter and are randomly oriented.

In order to achieve the uniform diameter distribution of nanotubes more experiments were conducted. Researchers have reported that the diameter distribution is more uniform for

low flow rate than for high flow rate.[20]The flow rate of carrier gas Ar was reduced by using pulsed flow instead of constant flow and keeping all other deposition conditions same. The Ar gas was pulsed between two flow rate values with pulse width (w) = 3 min during the complete deposition time. The high flow rate value was kept fixed at 200 sccm but the low flow rate value was varied as 0, 25, 50 and 100 sccm. The FESEM images of the resulted growth are shown in Fig. 3(a-d). The pulsed flow rates of carrier gas Ar during the complete deposition time are also plotted.

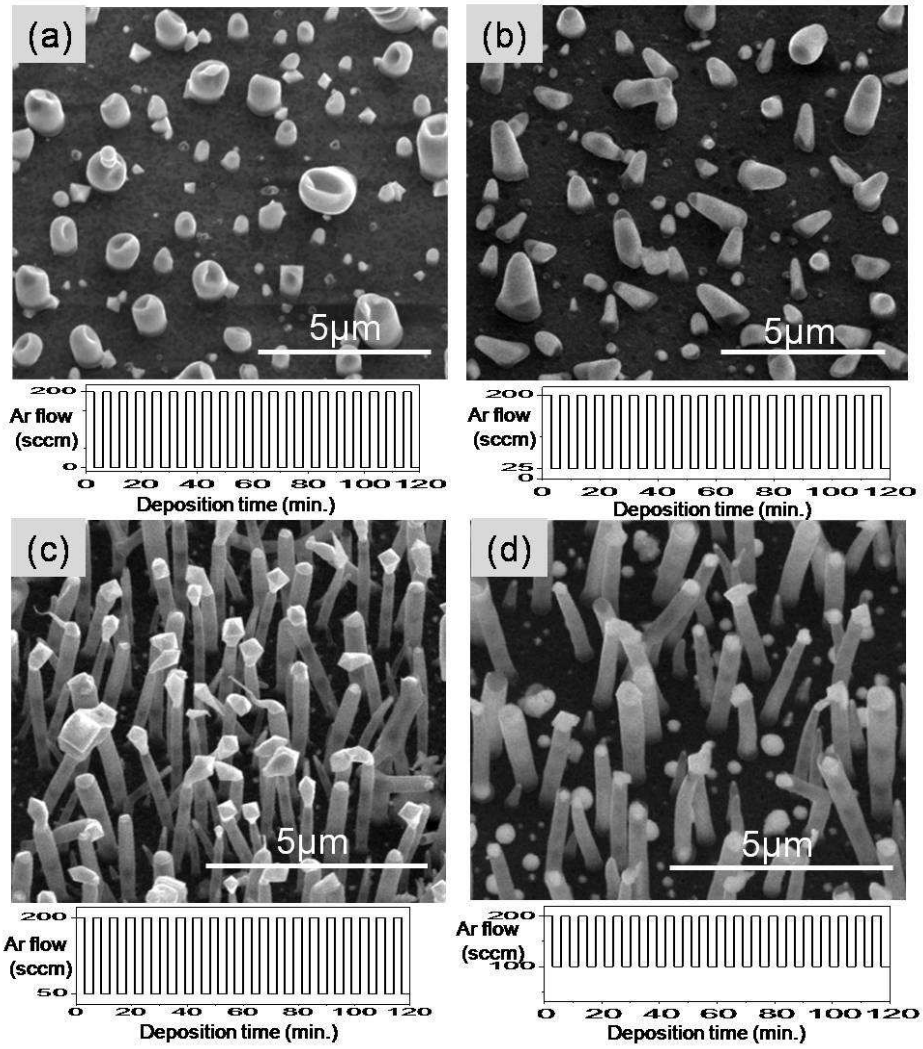

Fig. 3 FESEM micrograph of IO growth for pulsed Ar gas flow rates between (a) 200 to 0 sccm, (b) 200 to 25 sccm, (c) 200 to 50 sccm and (d) 200 to 100 sccm. The pulsed flow of Ar gas during complete growth time is shown graphically below the respective FESEM images.

When Ar gas flow rate was pulsed between 200 to 0 sccm the growth of nanotubes ceases due to interruption in the flow rate which lowers the concentration of reactant vapor species in the supersaturated catalyst alloy droplet and finally renders the growth of small nanodotsas shown in Fig. 3a. When Ar gas flow rate was pulsed between 200 to 25 sccm, a small reactive flux was transported to the substrate during lower flow rate cycle also. Hence, the growth didn't cease but appearedwith tapered tip as shown in Fig. 3b. For 200 to 50 sccm pulsed flow rate of Ar gas, vertically aligned nanotubes were observed as shown in Fig. 3c. The above experimental observations show that if we use pulsed mode of carrier gas flow then the lowerflow rate must be ≥ 50 sccm to continue the growth of IO nanotubes. From now, this sample will be referred to as IO-3. The average diameter (*d*) and length (*l*) of nanotubes were found to be 421 nm and 2.953 μm, respectively. We have synthesized samples with 200 sccm to 100 sccm pulsed flow rate of Ar gas also (sample A) and the FESEM image is shown in Fig. 3d. The average *d* and *l* of IO nanotubes are 546 nm and 2.562 μm, respectively. The enhancement in diameter for sample Ain comparison to sample IO-3 is due to the larger flux of reactant vapor species at the substrate as 100 sccm flow rate was used in place of 50 sccm. The length of nanotubes depends on the diameter. For larger diameter nanotubes, the incubation time was larger and hence, growth rate was small which resulted in nanotubes of relatively reduced length. Along with their dimensional change, the number density of IO nanotubes was also getting affected. There are some nucleation sites present in sample A where nanotubes were not grown. It shows that the maximum yield of nanotubes growth is possible only if, a sufficient amount of reactants vapor flux is localized in steady state on the substrate in the tube-in-tube system. Further experiments were done with Ar gas pulsed flow between 200 to 150 sccm and 200 to 175 sccm (not shown here), but no proper nanotubes were observed. Naturally, an optimization of pulsed flow rate in tube-in-tube CVD system is necessary to obtain vertically alignednanotubes growth with maximum

yield. The novel design of tube-in-tube CVD system plays an important role for vertical alignment of nanotubes. Inner quartz tube has its one end closed and precursor and substrate are placed inside the inner quartz tube. At elevated temperature, precursor evaporates and due to reduction of In_2O_3, the reactive species including In, In_2O and O_2 were transported by the carrier gas Ar to the substrate. Since, the other end of inner tube is closed, residual reactive species instead of ejecting out, returns back. Therefore inside the closed tube two directional flow exists; (1) flow of carrier gas directed towards right and (2) due to U-turn of reactive species directed towards left, as shown by arrows in Fig. 1. The net vertical flow as shown by red arrows in Fig. 1 is only possible if the horizontal components will cancel out with each other. Hence, the resulted vertical direction of local gas flow will determine the final growth direction of IO nanotubes. Geng*et al.*[21]reported the vertical growth of ZnO nanowires in closed tube-in-tube CVD system. Yan and co-workers[22] reported flow assisted alignment of silicon nanowires where the direction of the local gas flow determines the growth direction of nanowires. They used sandwich like configuration to enhance the local gas flow and showed that silicon nanowires growth was aligned along the flow direction of carrier gas flow. In the present study, it is found that the closed tube-in-tube system is not sufficient for obtaining vertically aligned IO nanotubes growth but the pulsed flow of Ar gas in tube-in-tube system is necessary to obtain the vertically aligned nanotubes.In the case of constant flow of Ar gas with 200 sccm flow rate, the obtained nanotubes are randomly oriented as shown in Fig. 2c. The growth obtained with pulsed flow of Ar gas with lower flow rate values as 0, 25, 50 and 100 sccm are shown Fig. 3. The pulsed flow rate of 200 to 25 sccm leads to tapered growth whereas pulsed flow of 200 to 100 sccm leads to low yield of nanotubes. The highest yield of vertically aligned nanotubes growth was obtained for pulsed flow rate of 200 to 50 sccm. These results indicate that a specific pulsed flow rate is required for vertical growth of IO nanotubes. In present case the 200 to 50 sccm pulsed flow rate is found to be sufficient to

cancel the forward and reverse horizontal flow in tube in tube system such that the net flow will be in vertical direction only. The resulted net vertical gas flow assists the nanotubes to grow in vertical direction. The above study confirms that what matters for growth of vertically aligned IO nanotubes is the local flux of reactive vapors near the substrate.

We have further studied the effect of Ar gas flow rate pulse width on the growth of IO nanotubes. Growth with different pulse widths of 0, 3, 4, 6, 7, and 8 min for the most appropriate pulsed flow between 200 to 50 sccm of Ar gas was carried out. The corresponding nanotubes samples were labelled as IO-0 (constant Ar flow of 200 sccm), IO-3 (w = 3 min), IO-4 (w = 4 min), IO-6 (w = 6 min), IO-7 (w = 7 min) and IO-8 (w = 8 min). We obtained nanotubes in every case but their dimensions and number density seems to get affected by different pulse width. The GAXRD spectra of all the IO nanotubes samples are shown in Fig. 4. It is found that the as-synthesized nanotubes are composed of cubic IO.

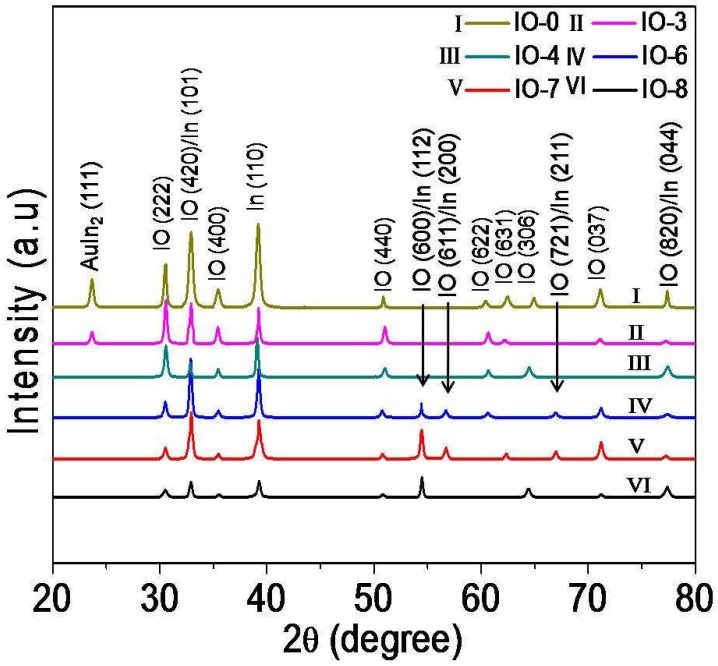

Fig. 4 GAXRD spectra of IO nanotube samples (IO-0, IO-3, IO-4, IO-6, IO-7 and IO-8) deposited with different Ar gas flow rate pulse width by vapor phase deposition method.

having lattice constant a = 10.12 Å (JCPDS: 76-0152). The peak at 2θ = 23.6˚can be assigned to $AuIn_2$ (111)[23] and the peaks at 2θ = 33.1˚, 39.2˚, 54.4˚, 56.1˚, 66.9˚ and 77.8˚can be assigned to IO (420)/In(101), In(110), IO(600)/In(112), IO(611)/In(200), IO(721)/In(211) and IO(820)/In(044), respectively. Fig. 5(a-f) shows tilted (30˚) FESEM images of as-synthesized IO tubular nanostructure arrays for w = 0, 3, 4, 6, 7 and 8 minutes.

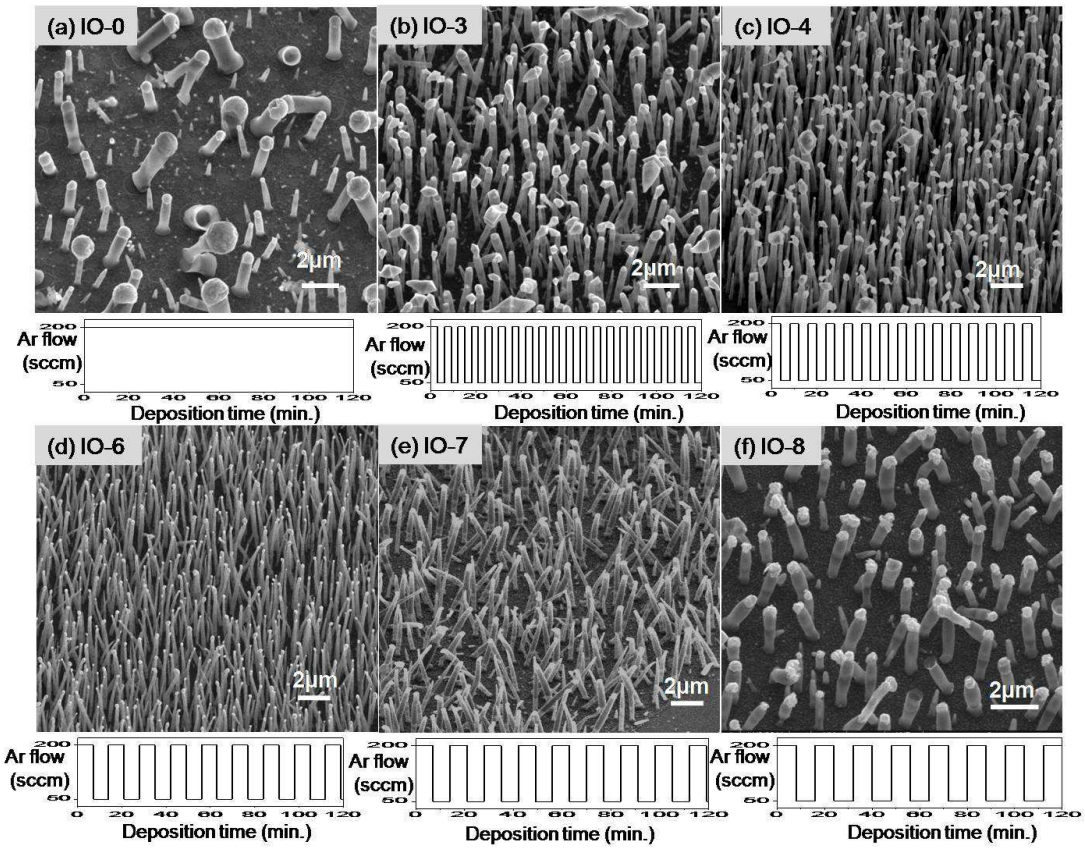

Fig. 5 FESEM micrograph of IO nanotubes grown with different pulse width of Ar gas flow rate in tube in tube CVD system. Image (a) to (f) shows the IO nanotubes of samples IO-0, IO-3, IO-4, IO-6, IO-7 and IO-8 grown with Ar gas flow rate pulse width 0, 3, 4, 6, 7 and 8 min, respectively. Pulsed Ar gas flow is represented graphically under the respective FESEM image.

It is clearly seen that nanotubes are vertically aligned but the dimensions and number density of nanotubes exhibits a strong dependence on w. The plot of average diameter (d) and length (l) of nanotubes as a function of w is shown in Fig. 6a. The d and l values of nanotubes are 621 nm and 2.021 μm for sample IO-0 where Ar gas flow rate was constant at 200 sccm. Now for w = 3 min (IO-3) the d and l values of obtained nanotubes are 421 nm and 2.953 μm,

when w = 4 min (IO-4) the d and l values of nanotubes are 349 nm and 3.643 µm and for w = 6 min (IO-6) the d and l values of nanotubes are 304 nm and 5.731 µm. The observed results reveal that with increase in $w$upto 6 min, the average diameter of nanotubes reduces with increase in average length of nanotubes. To find if this pattern of dimensional change will continue with further increasing w or not, we did more experiments with$w$ = 7 and 8 min. It was found that the average diameter of nanotubes increases and average length reduces. For$w$ = 7 min (IO-7) the d and l values of the nanotubes are 396 nm and 3.192 µm and for$w$ = 8 min (IO-8) the d and l values of nanotubes are 590 nm and 1.954 µm. It shows that the dimensional distribution of nanotubes critically depends on the pulse width of gas flow rate. Also, the observed number density of nanotubes are 4.3×10^7 cm^{-2} (sample IO-0), 8.2×10^7 cm^{-2} (sample IO-3), 12.7×10^7 cm^{-2} (sample IO-4), 12.9×10^7 cm^{-2} (sample IO-6), 6.4×10^7 cm^{-2} (IO-7) and 4.7×10^7 cm^{-2} (IO-8).It is important to notice that the growth of nanotubes is catalytically driven. Hence,the growth depends on the size of Au-In alloy droplet which decides the initial nucleation and further diameter and number density of IO nanotubes.

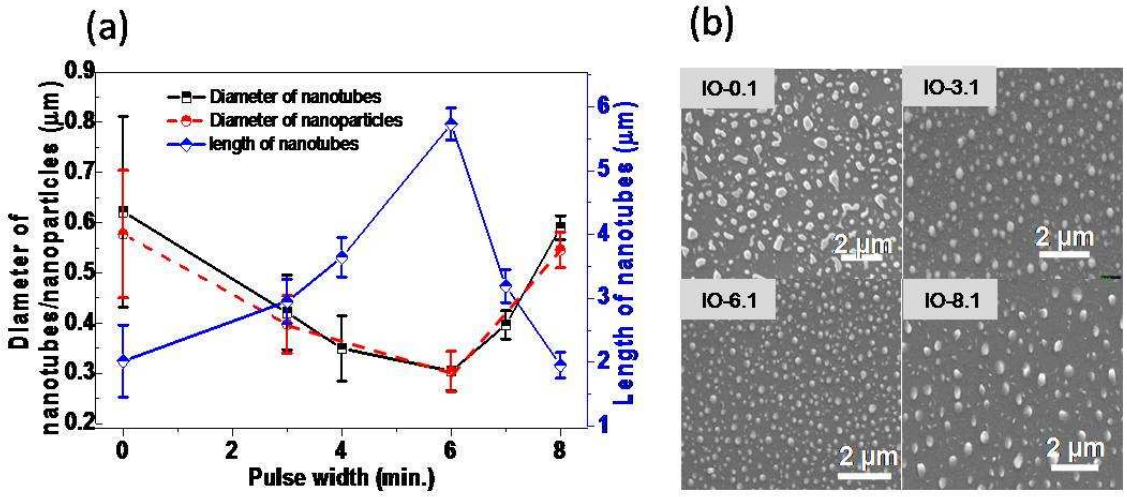

Fig. 6 (a) Diameter and length distribution of IO nanotubes as a function of pulse width of Ar gas flow rate. Dotted curve shows the diameter distribution of initial nucleation/nanoparticles as a function of pulse width for 10 min deposition time. (b) The SEM images of IO nanoparticles with pulse width of Ar gas flow rate for growth time of 10 min.

In order to demonstrate control over the diameter and number density of IO nanotubes with *w*, samples with different value of *w* = 0, 3, 6 and 8 min were grown. The total growth time was 10 min and all other deposition parameters kept similar to those used for vertical nanotubes growth. These four samples were labelled as IO-0.1, IO-3.1, IO-6.1 and IO-8.1, respectively and their FESEM images are shown in Fig. 6b. These samples were grown for 10 min to see the effect of *w* on initial nucleation site which further decides the diameter of nanotubes. The obtained nanoparticles showed diameter dependence on *w* as shown by dotted curve in Fig. 6a and follow the similar pattern as observed in grown nanotubes in different samples (IO-0 to IO-8). This phenomenon can be explained in term of the change in flux of indium rich reactive species which were transported by carrier gas on the substrate with different *w*. The estimation of nucleation with different *w* reveals that there are synthesis conditions in which the adatoms diffusion correlated with the time domain of modulation of reactive vapors flux. Based on this, we argue that by increasing *w* from 0 to 6 min results in lower flux transportation to the substrate. A small amount of reactive flux leads to decrease in the adatoms diffusion and coalescence of closely spaced nuclei which reduces the lateral growth. Therefore, the resulted nuclei are with lower diameter but their density increases due to decrease in lateral growth. By further increasing *w* upto8 min it is observed that the size of nuclei increases with decrease in number density and the size and number density of nanoparticles on samples IO-0.1 and IO-8.1 are nearly the same. It implies that for the pulsed flow of Ar gas with larger pulse width, the initial effect on nucleation is almost identical to the case of constant flow of Ar gas. For large pulse width of 7 and 8 min, the transportation of reactive flux in first cycle of Ar gas flow may be sufficient to decide the initial nucleation during growth. Hence, the initial nucleation size increases with decrease in number density for sample IO-7 and IO-8.Hahm*et al.*[20]reported that the size/diameter of nucleation site dependence on the gas flow rate which further controls the diameter distribution of carbon

nanotubes (CNTs). Also, the diameter distribution of CNTs is more uniform for low flow rate than for high flow rate. The length of the IO nanotubes is related with the diameter of nanostructures. The length is larger for smaller diameter nanostructures.Dhalluin*et al.*[24]have observed the growth rate dependence on diameter for silicon nanowires and shown that for thicker diameter (d >100 nm), nanowire length decreases with an increase in the diameter. On the basis of the present observations, It is found that the critical value of pulse width for growing vertically aligned nanotubes of maximum length of 5.731 μm is 6 min.

The typical TEM image of IO nanotube is shown in Fig. 7a. The TEM study reveals that all as-synthesized IO nanostructures are nanotubes in which some are partially filled with

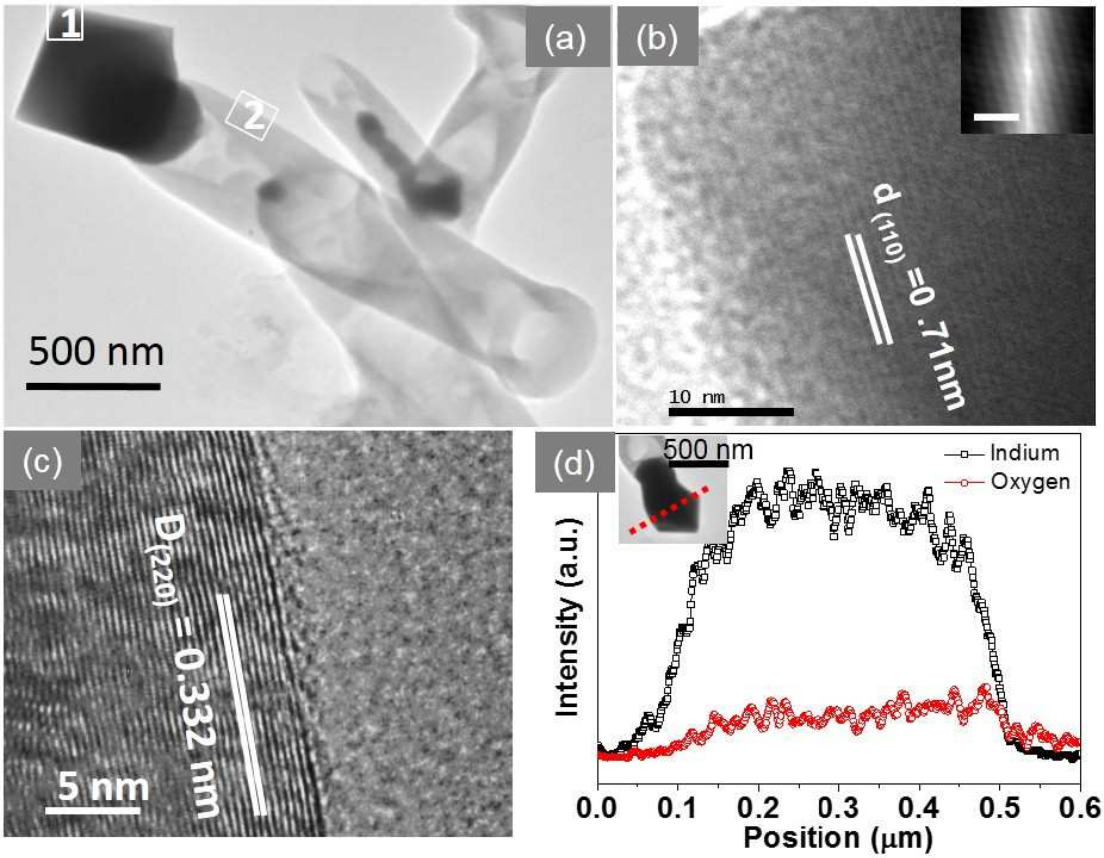

Fig. 7 (a) Typical TEM image of IO nanotube with octahedron at the tip. The open end of nanotube is encircled. (b) and (c) show the HRTEM images on tip and side wall of IO nanotube marked as position 1 and 2, respectively. (d) STEM-EDX along the radial direction of an IO octahedron on tip of IO nanotube. The inset shows a STEM image of the IO octahedron on tip of nanotube.

metallic indium. The outer diameter of nanotubes ranges from 300 nm to 623 nm and wall thickness varies from 50 nm to 110 nm. The nanotube diameter *d* is not uniform but decreases along the height. The transverse internal walls of hollow cavities inside the nanotubes are neither very smooth nor absolutely intact. The hollow cavities near the bottom region are triangular in shape but smooth and straight along the tube length. Fig. 7b and c show the HRTEM images of nanotube tip and sidewalls marked as position 1 and 2, respectively. The tip region shows lattice spacing of 0.71 nm, which corresponds to (110) lattice plane of cubic IOand lattice fringes of nanotube wall planes with lattice spacing of 0.328 nm, which corresponds to (220) lattice plane of cubic IO. The STEM-EDX measurement along the radial direction of octahedron at tip of nanotube is shown in Fig. 7d along with the STEM image in inset. The higher In:O ratio in the central region confirms that indium is encapsulated inside the IO octahedron on the tip of nanotubes. The spot EDX (not shown here) at nanotube wall and octahedron tip with In:O ratio is 0.6 and 1.5. It reveals that nanotubes' wall corresponds to stoichiometric In_2O_3 but octahedron tip is indium rich favouring the self-catalytic vapor liquid solid (VLS) growth mechanism for IO nanotubes.

The room temperature PLspectrum of vertically aligned IO nanotube arrays is shown in Fig. 8. The PL spectrum shows UV emission peak centered at 385 nm and broad visible emission with peakscentered at 537 nm and 630 nm. The UV emission is attributed to near band edge emission whereas the broad visible emission is contributing from more than one type of defects present in the indium oxide. Particularly, in our case, the vertically aligned indium oxide nanotubes were synthesized under reducing ethanol ambient, which results in oxygen deficient and indium rich reactive species during growth of IO nanotubes. Hence, defects like oxygen vacancy and indium interstitial formed easily during the growth of IO nanotubes. The green emission (537 nm) is attributed to oxygen vacancies and orange emission (630 nm) to indium interstitials.[25-27]

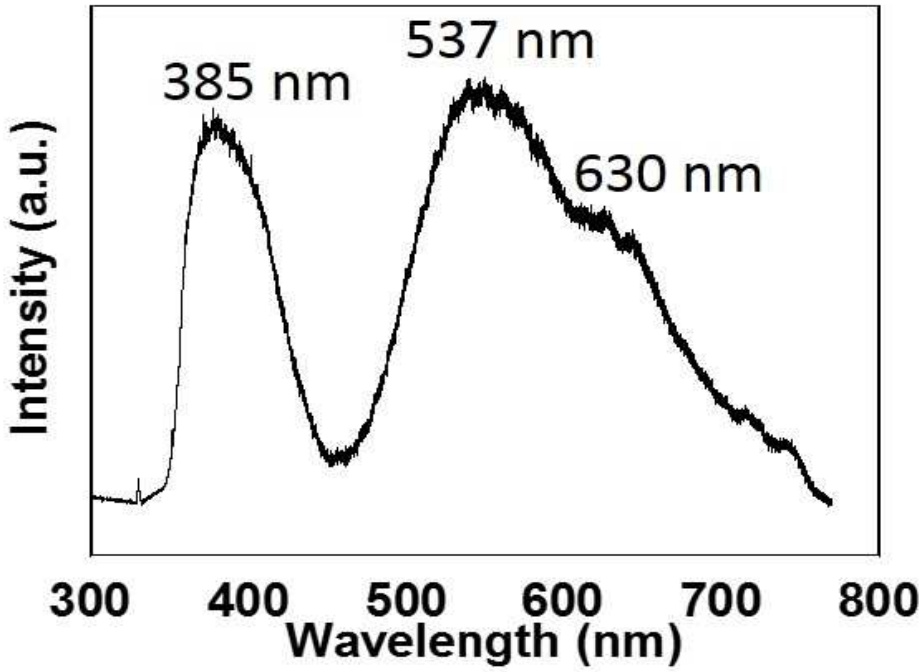

Fig. 8. The room temperature photoluminescence spectra from vertically aligned indium oxide nanotubes.

The Raman spectrum obtained from vertically aligned indium oxide nanotubes is shown in Fig. 9. The cubic IO belongs to space group I_a^3, T_h^7 having 22 Raman active modes (A_g, E_g and $T_g$symmetry) and 16 infra-red active modes (T_u symmetry). A few vibrations such as A_u and E_u are inactive in both infra-red and Raman measurements. The measured Raman spectra of IO nanotubes show peaks at 132.49, 306.79, 366.54, 495.22 and 626.56 cm^{-1} belong to the vibrational modes of body centered cubic (bcc) indium oxide. These values are in agreements with the previously reported Raman-mode frequencies for cubic indium oxide.[28, 29]

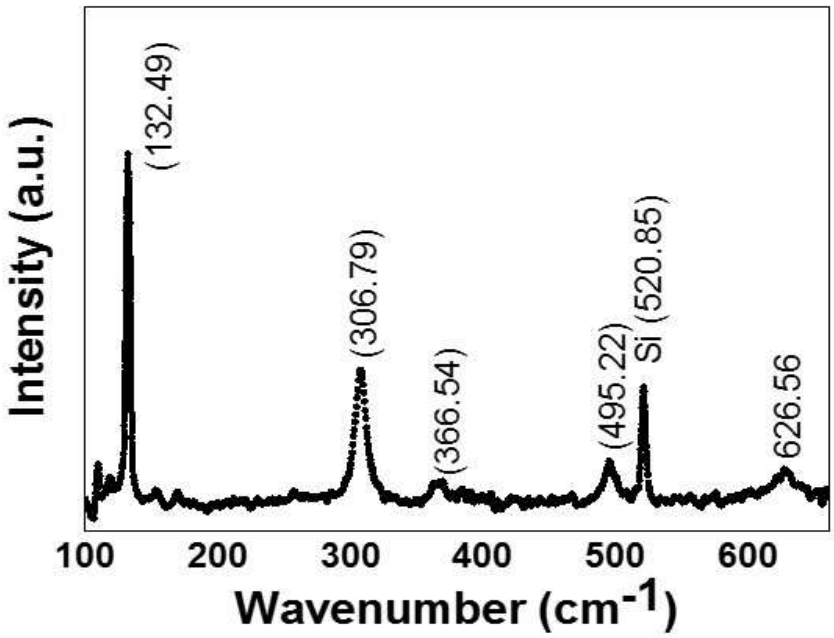

Fig. 9. The room temperature Raman spectra of vertically aligned indium oxide nanotubes.

The growth of IO nanotubes follows self-catalytic VLS mechanism. In order to understand why the as-synthesized IO nanostructures are hollow rather than solid, the shape of the tip of nanotubes has been examined carefully. The surface geometry of tip of nanotubes is closely related to the growth process. A schematic diagram of our proposed model is shown in Fig. 10 which describes a modified VLS mechanism for growth of IO nanotubes. When gold coated Si substrate was placed at 920 ℃ in the tube-in-tube CVD setup, the thin (~8 nm) Au film on Si substrate disintegrates into small Au dots which act as preferred sites for nucleation. Thermal evaporation of In_2O_3 involves gas phase transportation of In_2O, In, and O_2.[30, 31] Carbon mixed with In_2O_3 powder reduces it into oxygen deficient product In_2O and ethanol further reduces In_2O. This results in In rich active species.[32]

The reducing reactions taking place are as below:

Carbothermal reduction of indium oxide

$$In_2O_3(s) + C(s) \rightarrow In_2O(g) + CO_2(g) \quad (1)$$

Further reduction of reaction species due to ethanol ambient into an Indium rich ambient

$$3In_2O(g) + C_2H_5OH(g) \rightarrow 2CO_2(g) + 3H_2(g) + 6In(l) \quad (2)$$

The possible intermediate reactions involving reactant species, taking places during growth of IO in presence of oxygen are listed below:

$$In_2O(g) + O_2(g) \rightarrow In_2O_3(s) \quad (3)$$

$$3In_2O(g) \rightarrow 4In(l) + In_2O_3(s) \quad (4)$$

$$2In(l) + \frac{1}{2}O_2(g) \rightarrow In_2O(s) \quad (5)$$

$$In(l) + \frac{3}{2}O_2 \rightarrow In_2O_3(s) \quad (6)$$

Because of low melting point of indium (430 K at 1 atm) and low boiling point of In_2O (800 K at 1 atm), indium is present in liquid phase and In_2O in vapor phase. Indium from reactive species was adsorbed on catalytic centres and form Au-In compound(s). Stage II in Fig. 10 shows Au-In alloy droplet. The incoming vapors have large sticking coefficient at Au-In alloy droplets with liquid surface and therefore are the preferred adsorption site for incoming reactive vapors. Apparently, the dominating evaporating component was In_2O vapors, captured by the alloy droplets on the substrate which further decomposes into liquid indium and solid In_2O_3. After the Au-In liquid alloy became supersaturated, solid phase IO begins to diffuse out and would precipitate at the solid-liquid interface and nucleation starts as shown in stage III in Fig. 10. The geometry of the tip of the nanotubes is observed to change which may be due to mass transport of reactive species along the liquid droplet surface to the solid-liquid interface. The small changes in surface during transfer of material over the surface are in a direction to minimise the surface free energy.[33, 34] The droplet's radius of curvature contracts (may be at the time when droplet begins to phase separate from IO) as shown in

stage IV in Fig. 10, near solid-liquid interface to minimize the surface energy. The radius of curvature of the droplet is smaller at the bottom surface than at top surface, due to which anisotropic pressure appears on the alloy droplet. There is additional pressure at bottom surface because the pressure is inversely proportional to the radius of curvature. Further diffusion of reactive species increases the additional pressure and when it reaches at a critical point, the alloy droplet may squeeze out and leave a void behind (stage V, VI, VII in Fig. 10).

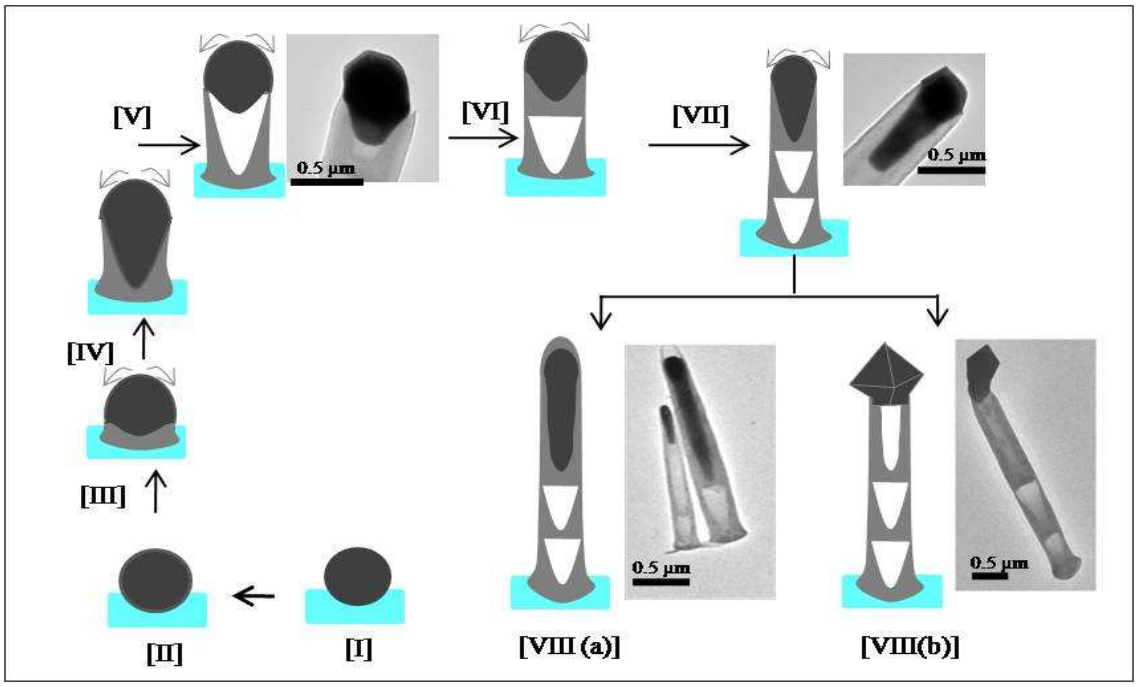

Fig. 10 Schematic illustration for the proposed growth mechanism of IO nanotubes. Different growth stages represent the alloy catalyst shape modification during growth. Curved arrows on the tip surface of nanotubes are representative for surface diffusion of reactive vapors. Typical TEM images are attached in support of respective growth stages.

The repetition of above mechanism results in hollow voids in the nanostructure. The mechanism can be understood as the effect of surface geometry of the alloy droplet, which was modified during adsorption and diffusion of reactive species during growth and is responsible for hollow voids. The diffusion of reactive species which mainly determines the growth rate occurs along the surface of the liquid alloy droplet rather than through the bulk. The surface diffusion may be preferred due to the relatively low flow rate of reactive species

in one end closed tube in comparison with the open ended tube. This can be explained on the basis of energy conservation in fluid dynamics. Due to the closed end of tube, the static pressure of reactive species increases in the tube which results as decrease in dynamic pressure as total pressure remains constant. The dynamic pressure is kinetic energy per unit volume and hence the flow rate of reactive species is relatively low in closed end tube system. Li *et al.*[35] also showed that lower flow rate of reactive vapor favours the formation of hollow nanostructures while disfavouring the growth of solid nanostructures. Indium present in alloy droplet gets consumed during growth with passage of time resulting in the reduction of diameter of nanotubes along its length. Also, Indium and IO have good wetting properties, due to which Indium may get sucked inside the core of nanotube due to the capillary effect in nanosize cavity. It may also be possible that during diffusion and condensation of the reactive species, the additional pressure on alloy droplet does not reach the critical point. In that case the alloy droplet may not squeeze out completely and results in partially filled IO nanotubes. When the alloy droplet gets completely sucked inside the tube, the resulted nanotubes have closed end tip, stage VIII (a) in Fig. 10. If the alloy droplet is not fully consumed during growth and finally appears on the tip of nanotubes, it results in octahedron morphology. With passage of time, precursor is consumed and further the reactive species get deficient in indium. The excess Indium on the tip of nanotubes may have tendency to re-evaporate and/or its surface oxidise to form IO octahedron because the system is at atmospheric pressure and there is continuous supply of oxygen from atmosphere. Growth of thermodynamically allowed crystallographic planes results in the form of octahedron structures at the tip of nanotubes as shown in stage VIII (b) in Fig. 10. Hao*et al.*[36]have mentioned that the growth rate (r) is perpendicular to three different low-indexed crystallographic planes and proportional to the surface energies, $\gamma\ \{111\} < \gamma\ \{100\} < \gamma\ \{110\}$. So, the growth rate (r)

perpendicular to {111} planes, i.e. r {111}, is comparatively slower and {111} planes have a tendency to appear as facets on the fast growing {110} and {100} planes.

Identical deposition of gold layer on Si substrate was used for all the samples but it was observed that pulsed gas flow rate with different *w* affect the catalyst size or initial nucleation, which further affects the dimensions and density of the finally grown nanotubes. Au play important role to initiate the growth as no such type of growth is observed on bare Si substrate. Pulsed flow of Ar gas in tube-in-tube CVD setup appeared to be important in controlling the vertical alignment and dimensions of nanotubes. Interestingly, it is observed that growth in tube-in-tube CVD setup with inner tube having both ends open was not vertical but randomly distributed.

Conclusions

In summary, vertical alignment of IO nanotubes can be achieved by a pulsed Ar gas flow in tube-in-tube CVD system without using any template or expensive epitaxial substrate. The dimensions of nanotubes can be controlled by using different pulse width of the carrier gas Ar. Our experimental results suggest thatgold catalyst plays an important role in the initial stages of growth of IO nanotubes and the nanotubes' diameter depends upon the size of alloy droplets. These vertically aligned IO nanotubes synthesizedby simple method of pulsed Argas flow in tube-in-tube CVD systemcould be beneficial for large number of applications such as photoelectrochemical cells, field emitters and solar cells.

Acknowledgements

The author KY kindly acknowledges CSIR, India for providing the senior research fellowship. We thank the Department of Science and Technology, India for providing a financial grant (grant number SR/S2/CMP-13/2010) and Nanoscale Research Facility (NRF) IIT Delhi, India for support.

References

1J. Gan, X. Lu, T.Zhai, Y. Zhao, S.Xie, Y. Mao, Y.Zhang, Y. Yang, Y.Tong, *J. Mater. Chem.*,2011,21, 14685.

2 Q.Wan, P.Feng, T. H.Wang, *Appl. Phys. Lett.*,2006, 89, 123102.

3 O. K.Varghese, M.Paulose, C. A. Grimes,*Nature Nanotechnology*,2009, 4, 592.

4 P.Nguyen, H.T.Ng, T.Yamada, M. K.Smith, J.Li, J.Han, M.Meyyappan, *Nano Lett.*,2004, 4, 651.

5 Q. Mu, H.Zhong, Y.Chen, G.Cao, Y. Xu, Q.Zhang, H.Wang, Y. Li, *Integr. Ferroelectr.*,2012, 135, 39.

6 Y. H.Chang, S. M.Wang, C. M.Liu, C. Chen, *J. Electrochem. Soc.*,2010, 157 (11), K236.

7 J. J. Martin, "Tunable, Highly Ordered TiO2 Nanotube Arrays on Indium Tin Oxide Coated PET for Flexible Bio-sensitized Solar Cells"U. S. Army Research Laboratory, Aberdeen Proving Ground, MD 2011.

8 A.Matsuda, S.Sreekantan, W. Krengvirat, *J. Asian Ceram. Soc.*,2013, 1, 203.

9 Y.Jun, J. H.Park, M. G.Kang, *Chem. Commun.*,2012, 48, 6456.

10 M.Zhong, M.Zheng, L.Ma, Y. Li,*Nanotechnology*,2007, 18,465605.

11 X. H.Li, W. M.Liu, H. L.Li, *Appl. Phys. A*,2005, 80, 317.

12 L.Shi, Y.Xu, Q.Li, *Nanoscale*,2010, 2, 2104.

13 H. P.Xiang, L.Chang, S.Chao, C. H. Ming, *Chin. Sci. Bull.*,2012,57, 187.

14 B. R.Mehta, F. E.Kruis,*Sol. Energy Mater. Sol. Cells*,2005, 85, 107.

15 G.Jo, W. K.Hong, J.Maeng, T. W.Kim, G.Wang, A.Yoon, S. S.Kwon, S.Song, T. Lee,*Colloids Surf. A*,2008, 313-314, 308.

16 D.-W.Kim, I.-S.Hwang, S. J.Kwon, H.-Y.Kang, K.-S.Park, Y.-J.Choi, K.-J. Choi, J.-G. Park,*Nano Lett*.,2007,7, 3041.

17 M.Curreli, C.Li, Y.Sun, B.Lei, M. A.Gundersen, M. E.Thompson,

396 C. Zhou, *J. Am. Chem. Soc.*,2005, 127, 6922.

397 18 S.Bianchi, E.Comini, M.Ferroni, G.Faglia, A.Vomiero, G.Sberveglieri,

398 *Sens. Actuators B*,2006, 118, 204.

399 19 B.Li, Y.Xie, M.Jing, G.Rong, Y.Tang, G.Zhang, *Langmuir*,2006, 22, 9380.

400 20 M. G.Hahm, Y. K.Kwon, E.Lee, C. W.Ahn, Y. J. Jung, *J. Phys. Chem. C*,2008,

401 112(44), 17143.

402 21 C.Geng, Y.Jiang, Y.Yao, X.Meng, J. A.Zapien, C. S.Lee, Y.Lifshitz,

403 S. T. Lee,*Adv. Func. Mater.*,2004, 14, 589.

404 22 C.Yan, T.Zhang, P. S. Lee,*Appl. Phys. A*,2009,94, 763.

405 23S. T.Jean, Y. C. Her,*Cryst. Growth Des.*,2010, 10, 2104.

406 24 F.Dhalluin, T.Baron, P.Ferret, B.Salem, P.Gentile, J.-C.Harmand,*Appl.*

407 *Phys. Lett.*,2010, 96, 133109.

408 25 H. J. Chun, Y. S. Choi, S. Y. Bae, J. Park, *Appl. Phys. A,* 2005,81, 539.

409 26 Y. Li, Y. Bando, D. Golberg, *Adv. Mater.,* 2003, 15, 581.

410 27 Y. R. Lyu, T. E. Hsieh, *Surf. Coat. Tech.,* 2013, 231, 219.

411 28 C. Y. Wang,Y. Dai,J. Pezoldt,B. Lu, T. Kups,V. Cimalla,O. Ambacher,

412 *Cryst. GrowthDes.,* 2008, 8, 1257.

413 29O. M.Berengue, A. D. Rodrigues, C. J.Dalmaschio,A. J. C.Lanfredi, E. R.Leite,

414 A. J.Chiquito, *J. Phys. D: Appl. Phys.,* 2010, 43, 045401.

415 30 R. P.Burns, G.DeMaria, J.Drowart, M. G.Inghram,*J. Chem. Phys.*,1963, 38, 1035.

416 31C. A.Pan, Ma, T. P. *J. Electrochem. Soc.*,1981, 128, 1953.

417 32 M. Kumar, V. N. Singh, B. R. Mehta, J. P. Singh,*Nanotechnology*, 2009, 20, 235608.

418 33 J. M. Blakely, *Progr. Mater. Sci.*, 1963, 10, 395.

419 34 H. Wang, G. S.Fischman, *J. Appl. Phys.*,1994, 76, 1557.

420 35 C. Li, Z. Liu, C.Gu, X.Xu, Y. Yang, *Adv. Mater.*, 2006, 18, 228.

421 36 Y.Hao, G.Meng, C. Ye, L. Zhang,*Cryst. Growth Des.*, 2005, 5, 1617.